ISSN 0023-1584, Kinetics and Catalysis, 2010, Vol. 51, No. 6, pp. 873–884. © Pleiades Publishing, Ltd., 2010.
Original Russian Text © V.V. Gorodetskii, A.V. Matveev, A.A. Brylyakova, 2010, published in Kinetika i Kataliz, 2010, Vol. 51, No. 6, pp. 902–913.

VIII INTERNATIONAL CONFERENCE ON MECHANISMS OF CATALYTIC REACTIONS

Experimental Study of Intermediates and Wave Phenomena in CO Oxidation on Platinum Metal (Pt, Pd) Surfaces

V. V. Gorodetskii, A. V. Matveev, and A. A. Brylyakova

Boreskov Institute of Catalysis, Siberian Branch, Russian Academy of Sciences, Novosibirsk, 630090 Russia
e-mail: gorodetsk@catalysis.ru

Received February 18, 2010

Abstract—The mechanism of catalytic CO oxidation on Pt(100) and Pd(110) single-crystal surfaces and on Pt and Pd sharp tip (~10^3 Å) surfaces has been studied experimentally by temperature-programmed reaction, temperature desorption spectroscopy, field electron microscopy, and molecular beam techniques. Using the density functional theory the equilibrium states and stretching vibrations of oxygen atoms adsorbed on the Pt(100) surface have been calculated. The character of the mixed adsorption layer was established by high resolution electron energy loss spectroscopy—molecular adsorption (O_{2ads}, CO_{ads}) on Pt(100)-*hex* and dissociative adsorption (O_{ads}, CO_{ads}) on Pt(100)-(1 × 1). The origin of kinetic self-oscillations for the isothermal oxidation of CO in situ was studied in detail on the Pt and Pd tips by field electron microscopy. The initiating role of the reversible phase transition (*hex*) ⟷ (1 × 1) of the Pt(100) nanoplane in the generation of regular chemical waves was established. The origination of self-oscillations and waves on the Pt(100) nanoplane was shown to be caused by the spontaneous periodical transition of the metal from the low-active state (*hex*) to the highly active catalytic state (1 × 1). A relationship between the reactivity of oxygen atoms (O_{ads}) and the concentration of CO_{ads} molecules was revealed for the Pd(110) surface. Studies using the isotope label $^{18}O_{ads}$ demonstrated that the low-temperature formation of CO_2 at 150 K is a result of the reaction of CO with the highly reactive state of atomic oxygen (O_{ads}). The possibility of the low-temperature oxidation of CO via interaction with the so-called "hot" oxygen atoms (O_{hot}) appearing on the surface at the instant of dissociation of O_{2ads} molecules was studied by the molecular beam techniques.

DOI: 10.1134/S0023158410060133

Investigation of the reactivity of adsorbed oxygen states was considered by Zamaraev [1] as a necessary step in establishing the mechanism of oxidative catalysis on metals. Present-day studies on the platinum metals show that even the simplest model reaction $CO + O_2$ described by the classical Langmuir–Hinshelwood mechanism, in which CO_2 molecules are synthesized from adsorbed oxygen atoms (O_{ads}) and molecules (CO_{ads}), is accompanied by the nonequilibrium energy distribution among the reaction products [2], anisotropy of the desorption of CO_2 molecules from the metal surface [2], the appearance of self-oscillations, and the formation of traveling chemical waves [3, 4]. In recent years, considerable attention has been focused on the reactivity of so-called "hot" oxygen atoms formed on the surface at the instant of dissociation of adsorbed molecules O_{2ads} [5]. It is assumed that the key role in the low-temperature CO oxidation on platinum metals is played by excited oxygen atoms (O_{hot}) [6]. The proposed mechanism is based on the experimental observation of a single peak of CO_2 at $T \sim 320$ K in the reaction of oxygen atoms with CO ($O_{ads} + CO_{ads} \longrightarrow CO_2$) on the Pt(111) surface under temperature-programmed reaction (TPR) conditions, whereas in the reaction of CO_{ads} with O_{hot} atoms ($O_{hot} + CO_{ads} \longrightarrow CO_2$) an additional low-temperature peak was observed at $T \sim 150$ K [7]. Our study of the mechanism for the reaction $O_{ads} + CO_{ads} \longrightarrow CO_2$ on the Pt(410) surface by the TPR and isotope label ($^{18}O_2$) methods showed the possibility of low-temperature CO oxidation proceeding at $T \sim 150$ K via another route, specifically, the CO_{ads} layer causes a decrease in the apparent activation energy (E_a) of the reaction due to changes in the type of coordination and the energy of binding of the adsorbed oxygen atoms to the surface [8].

The great interest in self-oscillatory phenomena over metal surfaces is largely caused by the possibility of performing the catalytic processes more efficiently using unsteady-state operation. In the oscillating regime, the reaction medium periodically affects the catalytic properties of metal surfaces [1, 9]. Different mechanisms of the appearance of self-oscillations and waves were discovered and studied. These are a periodical change in the structure of active sites during the phase transition ($CO + O_2$/Pt(100): (*hex*) ⟷ (1 × 1)), the modification of the surface via the formation of a subsurface oxygen layer ($CO + O_2$/Pd(110)) that were

found on Pt(100), Pt(110), Pd(110) single crystals [3, 4]. The use of spatially resolved (~1 μm) photoemission electron microscopy made it then possible to discover the formation of traveling waves on the Pt and Pd single crystal surfaces [3, 4]. Unlike single crystals, the metal/support catalysts usually consist of nano-sized metal particles on which different crystallographic nanoplane structures are exposed. Passing to the nanolevel was performed for the first time in our studies by field electron microscopy (FEM) and field ion microscopy (FIM) with a spatial resolution of ~5–20 Å. Sharp monocrystalline Pt tips with sizes of $\sim 10^3$ Å were used as samples in these studies. In CO and H_2 oxidation, we observed in situ the formation of regular traveling waves initiated by the reversible phase transition (*hex*) $\leftrightarrow$ (1 × 1) of the Pt(100) nanoplane [9–12].

This brief review includes some results obtained by methods of TPR, FEM, temperature desorption spectroscopy (TDS), high resolution electron energy loss spectroscopy (HREELS), molecular beam (MB), and isotope label ($^{18}O_2$). The main attention in our studies was given to determination of the reactivity of the molecular and dissociated oxygen species adsorbed on the Pt(100) and Pd(110) single crystals in the low-temperature formation of CO_2 molecules and to investigation of the mechanism of origination of self-oscillations and chemical waves in CO oxidation in situ on the nanoplanes of sharp Pt and Pd tips. Using the techniques of density functional theory (DFT), the equilibrium states and stretching vibrations of oxygen atoms, adsorbed on the Pt(100) have been calculated depending on the surrounding of the metal atoms.

EXPERIMENTAL

Experimental studies by the HREELS, TPR, and molecular beam methods were carried out in the vacuum chamber of a VG ADES 400 electron spectrometer ($P_{res} < 5 \times 10^{-11}$ mbar). The energy loss spectra with a resolution of ~70–90 cm^{-1} (9–11 meV) were obtained in the electron beam specular reflection mode at an electron kinetic energy of ~2.5 eV and an incident angle of ~45° with respect to the surface normal. HREELS peak intensities in the electron energy loss spectra were determined relative to the intensity of the elastically reflected peak. TPR spectra were recorded on a VG QXK 400 quadrupole mass at a linear heating rate of 3–10 deg/s with simultaneous detection of ten different masses. The clean surface of the single crystals was obtained by bombardment with Ar^+ ions followed by annealing in oxygen and in a vacuum up to 1200 K. The cleanness of the surface was monitored as the appearance of the diffraction pattern (1 × 1) for the single crystals Pd(110) and Pt(100)-(1 × 1) and (5 × 20) for the reconstructed surface of Pt(100)-*hex*. The temperature was measured with a chromel–alumel thermocouple spot-welded to the side surface of the single crystal. The gases CO and O_2 and the oxygen isotope $^{18}O_2$ of spectral purity were used in experiments. The experimental procedure was described earlier [13]. Gas injection into the chamber as a collimated molecular beam was controlled by using a capillary array dozer [14],which made it possible to create a high local pressure on the single crystal surface. FEM studies were carried out using a separate ultrahigh-vacuum setup ($P_{res} < 10^{-10}$ mbar) under flow reactor conditions with visual observation of the tip (Pt, Pd) surface in situ. The pressure of the reaction medium was maintained at ~5×10^{-4} mbar and was monitored with a quadrupole mass spectrometer. The preparation of sharp tips and cleaning of the surface by "field desorption," as well as other experiments were described in detail elsewhere [15, 16].

RESULTS AND DISCUSSION

Steady-State Reaction

CO oxidation under steady state conditions over palladium proceeds via a Langmuir–Hinshelwood reaction and consists of the following elementary steps:

$$1.\ CO + * \leftrightarrow CO_{ads},$$
$$2.\ O_2 + 2* \rightarrow 2\,O_{ads},$$
$$3.\ CO_{ads} + O_{ads} \rightarrow CO_2 + 2*,$$

where * is an adsorption site. This mechanism is presently a subject of wide fundamental research, especially in the region of low temperatures. The rate of CO oxidation on the Pd(110) single crystal was measured under steady-state conditions in the temperature range from 180 to 850 K using the molecular beam techniques (Fig. 1a). At the instant of admission ($t_0 = 0$) of the CO + O_2 mixture as a beam with an intensity of 0.03 ML/s (1 ML = 1 monolayer ≅9.4×10^{14} molecules/cm^2) onto the clean surface of the metal, CO_2 molecules initially form "jumpwise," and this is followed by the steady-state occurrence of the reaction, which is established within a temperature-dependent period t. In the low-temperature region T ~ 180–350 K, a slow initial increase in the rate of CO_2 formation (solid curve) is observed. The maximum value is reached after t ~ 20–50 s, and then the rate decreases and the steady state is reached at t ~ 130 s. The character of CO_2 formation changes sharply at medium temperatures T ~ 420–550 K: at the moment t_0, the intensity of the CO_2 signal grows stepwise and the steady state is reached simultaneously. The initial rate of formation of CO_2 molecules decreases in the high-temperature region $T > 550$ K. The initial and steady-state rates of formation of CO_2 molecules at different temperatures are compared in Fig. 1b. It can be seen that the admission of the CO + O_2 molecular beam onto the clean metal surface is characterized by the formation of CO_2 molecules as two maxima: at T ~ 230 and ~450 K (solid curve). The steady-state occurrence of the reaction (dashed line) is characterized by one maximum at T ~ 390 K. It is likely that the

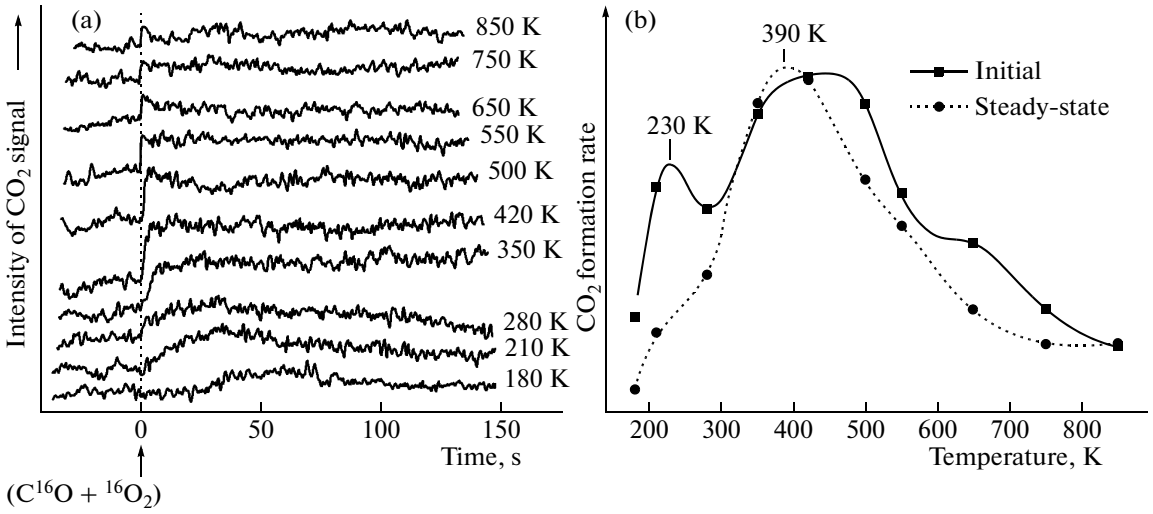

Fig. 1. (a) Time evolution of the rate of CO_2 formation during the impingement (shown by arrows) of a $(C^{16}O + {}^{16}O_2)$ molecular beam of intensity ~0.03 ML/s onto the Pd(110) clean surface. (b) Comparison of the temperature dependences of the initial (0 s) and steady-state rate (130 s) of CO_2 formation.

absence of the low-temperature maximum (230 K) during the steady-state reaction rate is due to the specific composition of the adsorption layer (θ_{CO}/θ_O ratio), which contains a high concentration of CO_{ads} molecules.

Low-Temperature Oxidation of CO on the Pd(110) Surface

At present, the possibility of the low-temperature formation of CO_2 on Pd and Pt via the following two independent routes is discussed in the literature: reaction of CO_{ads} with "hot" oxygen atoms resulting from the dissociation of O_{2ads} molecules (R_1), and reaction of CO_{ads} with weakly bound, high-reactivity atomic oxygen formed from the strongly bound O_{ads} species as affected by the CO_{ads} layer (R_2) [5–8]. The molecular beam and ${}^{18}O_2$ label methods were used to study the relationship between the low-temperature formation of CO_2 molecules and the reactivity of the different adsorbed oxygen species on the Pd(110) surface, namely, "hot" ($^{16}O_{hot}$) and atomic ($^{18}O_{ads}$) oxygen. The schemes of the CO_2 formation routes are shown in Fig. 2a, one involving "hot" oxygen atoms ($^{16}O_{hot}$) formed at the instant of dissociation of $^{16}O_{2ads}$ molecules, and the other involving preadsorbed oxygen atoms ($^{18}O_{ads}$).

Since $E_{act}(R_1) \ll E_{act}(R_2)$, according to the scheme presented, the formation of "hot" $^{16}O_{hot}$ atoms upon the dissociation of $^{16}O^{16}O$ molecules should be accompanied by a stepwise change in the intensity of the formation of $C^{16}O^{16}O$ molecules when a mixture of the reactants $C^{16}O + {}^{16}O_2$ impinges onto palladium surface precovered with a $^{18}O_{ads}$ layer at the instant of molecular beam opening. (The $C^{16}O + {}^{16}O_2$ mixture is impinged directly onto the $^{18}O_{ads}$/Pd(110) surface as a collimated molecular beam with the simultaneous detection of the reaction products—$C^{16}O^{16}O$ and $C^{16}O^{18}O$.)

The experimental procedure includes two successive stages. At the first stage (to create the isotope label, $\theta(^{18}O_{ads})$), ${}^{18}O_2$ oxygen was preadsorbed on the Pd(110) surface at 140 K at an exposure of ~0.8 L (1 L = 1.3×10^{-6} mbar s), which was followed by heating to ~300 K. This was accompanied by surface reconstruction from the structure (1 × 1) to the structure (1 × 2). Isolated "islands" of $^{18}O_{ads}$ corresponding to the coverages $\theta_O \sim 0.5$ ML form on the surface under these conditions (Fig. 2b). At the second stage, the reaction mixture with the light oxygen isotope ($C^{16}O + {}^{16}O_2$ (2 : 3)) was impinged onto the surface as a molecular beam with an intensity of 0.03 ML/s. The rates of $C^{16}O^{16}O$ formation (R_1) and $C^{16}O^{18}O$ formation (R_2) were simultaneously recorded at the instant of beam opening.

The experimental data on the rate of formation of molecules $C^{16}O^{16}O$ and $C^{16}O^{18}O$ upon the admission of the molecular beam ($C^{16}O + {}^{16}O_2$) onto the $^{18}O_{ads}$/Pd(110) surface are shown in Fig. 2c. The reaction rate was measured at $T = 300$ K. The upper spectrum corresponds to the reaction $^{18}O_{ads} + C^{16}O_{ads} \longrightarrow C^{16}O^{18}O_{gas}$, and the lower spectrum corresponds to the reaction $^{16}O_{ads} + C^{16}O_{ads} \longrightarrow C^{16}O^{16}O_{gas}$. It can be seen that CO oxidation at 300 K proceeds only via the second route, involving the atomic state of $^{18}O_{ads}$, without a noticeable participation of the first route, whereby $C^{16}O^{16}O$ molecules would be formed. These results led us to the following conclusions: (1) at 300 K the preadsorbed $^{18}O_{ads}$ atoms are highly reactive ($^{18}O_{ads} + CO_{ads} \longrightarrow CO_2$); (2) no direct evidence was obtained for the formation of "hot" oxygen atoms capable of

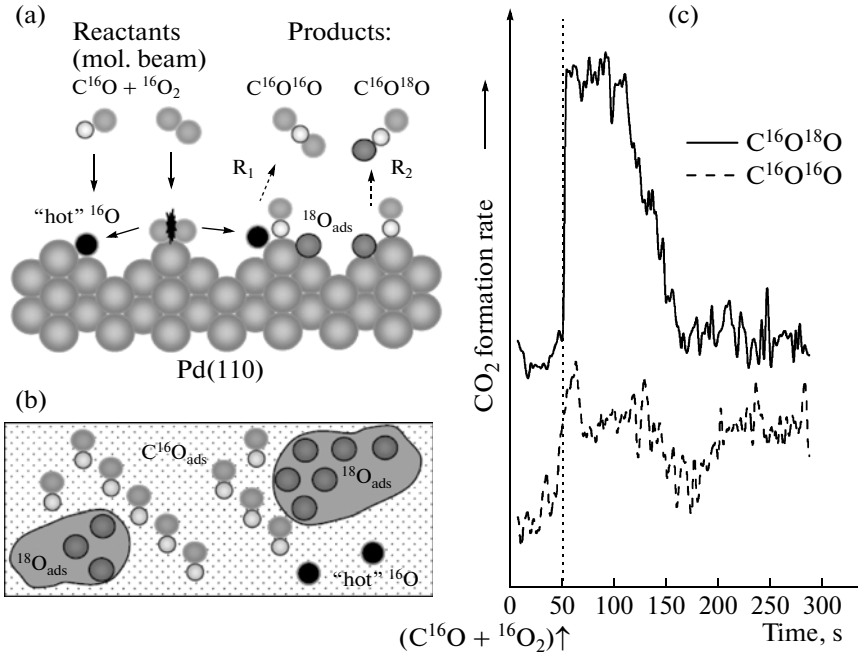

Fig. 2. (a) Reaction routes (R_1, R_2) for the formation of CO_2 molecules involving (R_1) the "hot" oxygen atoms $^{16}O_{hot}$ (blackened) formed at the instant of dissociation of $^{16}O_{2ads}$ molecules and (R_2) the preadsorbed layer of the $^{18}O_{ads}$ oxygen isotope; (b) state of the surface after $C^{16}O + {}^{16}O_2$ impinging on Pd(110) with the isolated O_{ads} "islands" (for details, see text); (c) formation rate of CO_2 ($C^{16}O^{16}O$ and $C^{16}O^{18}O$) upon impinging the reaction mixture ($C^{16}O + {}^{16}O_2$) in the molecular beam regime on a Pd(110) surface precovered with $^{18}O_{ads}$ ($\theta_O \sim 0.5$ ML). The intensity of the beam ($CO + O_2$) is 0.03 ML/s; $T = 300$ K. The upper spectrum refers to the reaction $^{18}O_{ads} + C^{16}O_{ads} \longrightarrow C^{16}O^{18}O$, and the lower spectrum corresponds to the reaction $^{16}O_{ads} + C^{16}O_{ads} \longrightarrow C^{16}O^{16}O$.

oxidizing CO ($^{16}O_{hot} + CO_{ads} \longrightarrow CO_2$) according to the reaction scheme presented in Fig. 2a.

The strong effect of the CO_{ads} layer on the reactivity of oxygen atoms (O_{ads}) was studied by the TPR method. The TPR spectra characterizing the rate of CO_2 formation in the reaction $CO_{ads} + O_{ads}$ on the Pd(110) surface at different concentrations of CO_{ads} molecules are shown in Fig. 3. The procedure of preparation of a coadsorption layer from oxygen atoms (O_{ads}) and CO_{ads} molecules includes oxygen adsorption at 120 K (0.3 L) followed by heating in a vacuum to 200 K in order to remove O_{2ads} molecules. After cooling to 120 K, CO was adsorbed on the surface. For surface coverages of $\theta_O \sim 0.25$ ML and $\theta_{CO} \sim 0.2$ ML (5 L CO), heating (3 K/s) of the mixed layer of O_{ads} atoms and CO_{ads} molecules in the T range from ~120 to 600 K is accompanied by the appearance of two CO_2 peaks at 350 and 410 K. For high coverages of $\theta_{CO} \sim 1$ ML (30 L CO, $\theta_O = \text{const} \sim 0.25$ ML), the reaction is shifted to the low-temperature region ($T < 300$ K) and is characterized by the intensive formation of CO_2 molecules between 150 and 280 K.

The results obtained indicate the high reactivity of O_{ads} atoms in the low-temperature region from 150 to 200 K. It is likely that the high local concentration of CO_{ads} molecules in the mixed layer ($CO_{ads} + O_{ads}$) promotes the transition of oxygen atoms from the strongly bound threefold hollow site state (Pd_3–O_{ads}) to the twofold bridge state (Pd_2–O_{ads}) with a lower bond energy, which explains the observed increase in the reactivity of the O_{ads} atoms and is consistent with the theoretical calculations [8, 17].

Low-Temperature CO Oxidation on the Pt(100) Surface

The "phase transition" model based on the interrelation between the CO oxidation rate self-oscillations and the reversible phase transition *hex* $\longleftrightarrow$ (1 × 1) of the Pt(100) single crystal surface was suggested by Ertl [3, 4]. It was shown by FEM that the Pt(100) nanoplane under self-oscillation conditions is reversibly transformed into different structures, namely, the low-activity surface phase (*hex*) and high-activity surface phase (1 × 1) [18]. Figure 4a presents the model of the upper layer of the Pt(100) surface with the (*hex*) structure, which is 20% denser than the upper layer of the unreconstructed Pt(100)-(1 × 1) surface. At 300 K, CO adsorption on (*hex*) is accompanied by the backward reconstruction of the Pt(100) surface yielding $CO_{1\times1}$ islands. The phase transition (*hex*) $\longrightarrow$ (1 × 1) induced by CO adsorption generates structural atomic

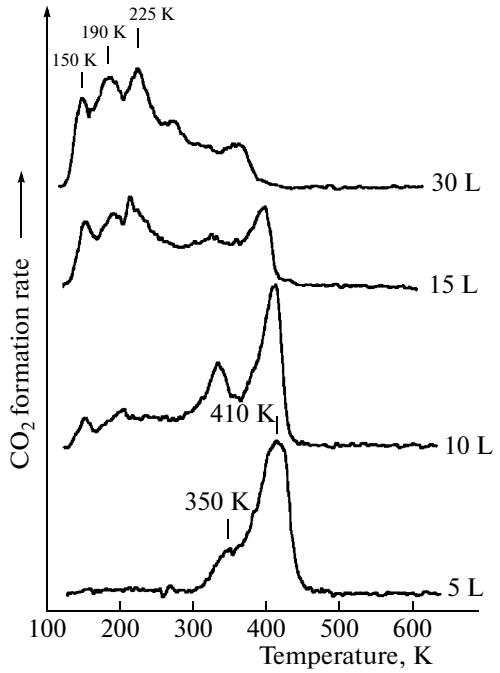

Fig. 3. TPR spectra for the reaction $CO_{ads} + O_{ads}$ in the coadsorption layer on the Pd(110) surface at different exposures to CO (5–30 L) at $\theta_O = \text{const} \sim 0.25$ ML; $T_{ads} =$ 120 K; heating rate of 3 K/s.

cluster–type defects in the islands by ejecting the platinum atoms to the upper layer (Fig. 4c). The low activity of the (*hex*) phase in CO oxidation is due to the low sticking coefficient: $S_0(O_2) \sim 10^{-3}$. The high activity of the (1 × 1) phase is due to both the high $S_0(O_2)$ value ($\sim 10^{-1}$) and the formation of the reactive oxygen species O_{ads} on defects of the (100) surface during the (*hex*) ⟶ (1 × 1) transition.

The reactivities of the intermediates in the coadsorption layer (O_{ads}, O_{2ads}, CO_{ads}) on the (*hex*) and (1 × 1) surface structures are compared in Figs. 4 and 5. According to HREELS data, the adsorption of O_2 (30 L) on Pt(100)-*hex* at 90 K results in the formation of the molecular peroxide species O_{2ads}^{2-} with stretching vibration frequencies of $\nu(O{-}O) = 940$ and $\nu(Pt{-}O_2) = 380$ cm^{-1} (Fig. 4a). Heating of the O_{2ads} layer in the $T \sim 90$–250 K range induces oxygen desorption into the gas phase at $T_{des} \sim 150$ K (Fig. 4b). The reactivity of the molecular species (O_{2ads}, CO_{ads}) was studied in the mixed adsorption layer, which at the initial stage (CO adsorption, 300 K, 1 L) consisted of isolated $CO_{1\times1}$ islands. The latter are presented as a model in Fig. 4c. The subsequent adsorption of O_2 at 90 K (10 L) on the free (*hex*) phase of Pt(100) results in the formation of the peroxide species O_{2ads}^{2-} [19]. The temperature-programmed desorption spectra of CO_2, CO, and O_2 from the mixed layer of $CO_{1\times1}$ and O_{2ads} are shown in Fig. 4c. Between 90 and 700 K, desorption occurs only from the molecularly adsorbed states of oxygen ($T_{des} \sim 140$ K) and carbon oxide ($T_{des} \sim$ 510 K). Probably, the absence of the evolution of CO_2 molecules is a consequence of the following factors: the catalytic activity of the Pt(100)-*hex* surface is low and the $CO_{2ads} + O_{2ads}$ reaction (molecular mechanism) cannot occur at low temperatures. It is likely that the layer of $CO_{1\times1}$ molecules both inside the (1 × 1) islands and on structural defects along the perimeter of the islands is characterized by a large θ_{CO} value (0.5 ML) [13], which rules out the presence of

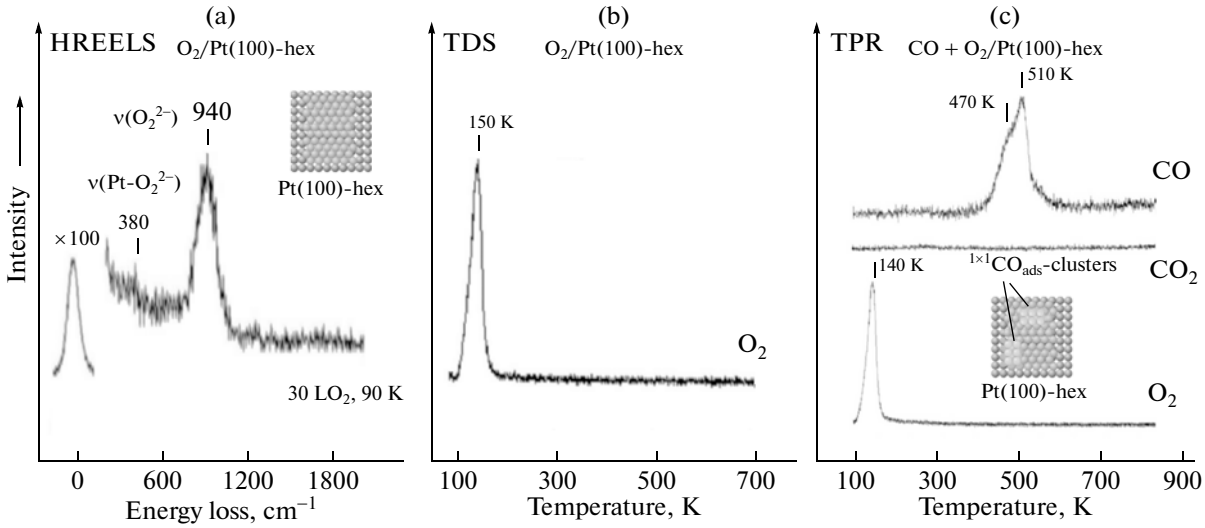

Fig. 4. (a) HREELS, (b) TDS, and (c) TPR spectra for the Pt(100)–*hex* surface: (a) electron energy loss spectrum after O_2 adsorption (30 L) at 90 K, (b) desorption spectrum of the O_{2ads} layer, and (c) desorption spectra of CO, O_2, and CO_2 during heating of the mixed adsorption layer of O_{2ads} and CO_{ads}, obtained by the sequential adsorption of CO (300 K, 1 L, $CO_{1\times1}$ islands) and O_2 (90 K, 10 L); heating rate of 10 K/s.

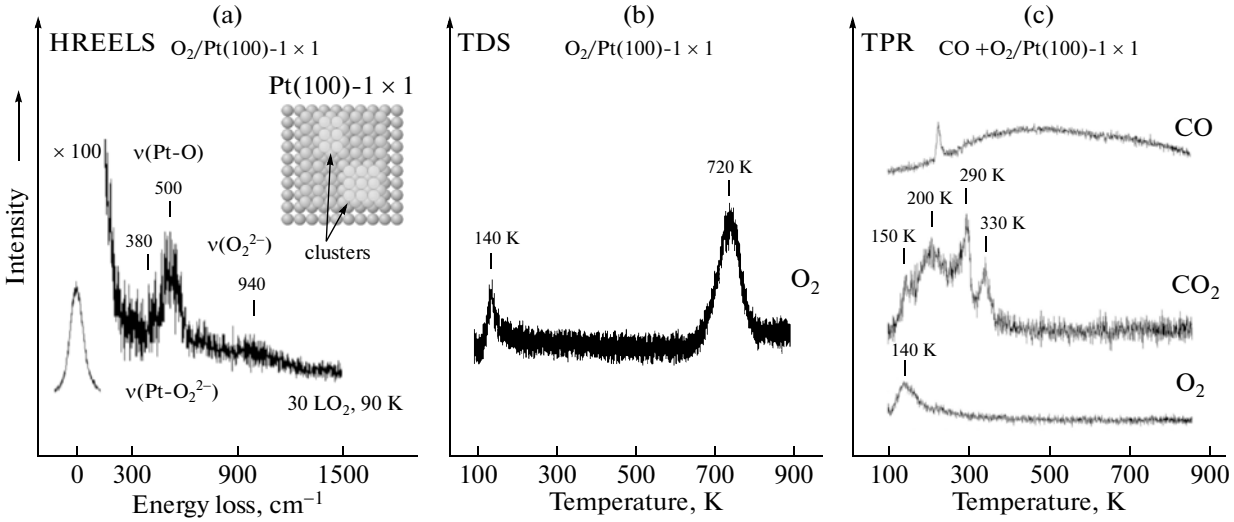

Fig. 5. (a) HREELS, (b) TDS, and (c) TPR spectra for the Pt(100)-(1 × 1) surface: (a) electron energy loss spectrum after O_2 adsorption (30 L) at 90 K, (b) desorption spectrum of the $O_{2ads} + O_{ads}$ layer, and (c) desorption spectra of CO, O_2, and CO_2 during heating of the mixed adsorption layer of $O_{2ads} + O_{ads} + CO_{ads}$, obtained by the sequential adsorption of O_2 (90 K, 30 L) and CO (90 K, 10 L); heating rate of 10 K/s.

free sites necessary for the dissociation of molecular oxygen.

At 90 K (30 L), the clean unreconstructed surface Pt(100)-(1 × 1) prepared according to a known procedure [20] adsorbs oxygen as the molecular peroxide species O_{2ads}^{2-} with stretching frequencies of ν(O–O) = 940 and ν(Pt–O_2) = 380 cm^{-1} (Fig. 5a). The dissociative adsorption of O_2 is simultaneously observed, which yields a layer of atomic oxygen characterized by a vibration frequency of ν(Pt–O) = 500 cm^{-1}. The desorption spectrum presented in Fig. 5b contains the low-temperature peak (140 K) of the molecular state of oxygen and a high-temperature peak (720 K), which is a result of the recombination of adsorbed oxygen atoms. The desorption spectra of CO_2, CO, and O_2 from the mixed adsorption layer ($CO_{ads} + O_{ads} + O_{2ads}$) are shown in Fig. 5c. The desorption of dioxygen at 140 K in the $CO_{ads} + O_{2ads}$ reaction indicates the absence of the molecular mechanism of CO_2 formation on the unreconstructed surface (1 × 1). However, the low-temperature formation of CO_2 molecules observed as four desorption peaks at 150, 200, 290, and 330 K in the $CO_{ads} + O_{ads}$ reaction shows the high catalytic activity of the Pt(100) surface with the (1 × 1) structure.

Coordination modes, equilibrium distances (r_0) from the surface, and vibrational frequencies ($\nu_\perp$) of the O_{ads} atoms on the Pt(100)-(1 × 1) surface at θ = 1 ML, calculated by the DFT technique

Coordination mode	r_0, Å	$\nu_\perp$, cm^{-1}
On–top	1.80	750
Bridge	**1.33**	**650**
Hollow	0.85	380

DFT Calculations

Using the DFT technique, the equilibrium distances (r_0) and stretching frequencies (ν) of O_{ads} atoms (θ_O = 1 ML) adsorbed on the Pt(100) surface have been calculated depending on the surrounding of the metal atoms at the active site. We have employed a three-layer slab [16] for simulation of the Pt(100)-(1 × 1) surface. Adsorbed oxygen atoms can occupy the following three states: fourfold hollow site, twofold bridge site, and on-top. The calculations were performed using the ADF2003–BAND and ESPRESSO-3.1 programs.

The calculated equilibrium distances and stretching frequencies of oxygen at θ_O = 1 ML (table) suggest that the position of the oxygen atom in the bridge structure is more favorable than its position in the on-top or hollow structure.

The experimental and theoretical data concerning the possibility of dissociation of O_2 molecules on the (*hex*) and (1 × 1) phases, the character of the low-temperature oxidation of CO_{ads} molecules on (1 × 1), the coordination number of oxygen atoms on (1 × 1), and the effect of the CO_{ads} layer on the reactivity of the O_{ads} atoms make it possible to chemically substantiate the mechanism of wave phenomena in the CO + O_2 reaction on the Pt(100) surface based on the reversible phase transition Pt(100)-(*hex*) ⟷ (1 × 1).

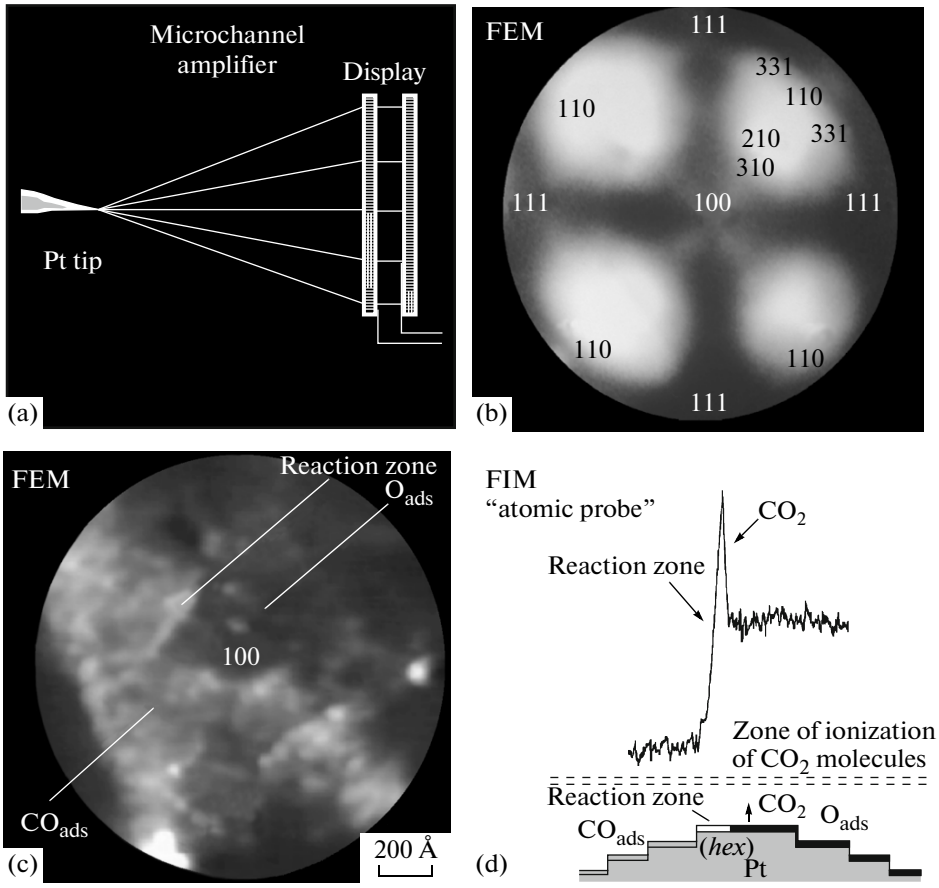

Fig. 6. (a) A schematic representation of the magnification process in the field electron microscope; (b) a field electron image of the Pt tip surface with a radius of ~700 Å and orientation [100]: $V_{FEM} = -2.5$ kV, $F = 0.3$ V/Å; (c) field electron image of the same surface of the Pt tip with an O_{ads} layer (dark spot) adsorbed on the (100) nanoplane surface obtained in situ under conditions of traveling wave formation in the reaction $CO + O_2$: $T = 450$ K, $P(O_2) = 1.5 \times 10^{-4}$ mbar, $P(CO) = 1 \times 10^{-5}$ mbar; (d) CO_2^+ intensity on the CO_{ads}-side, O_{ads}-side of the reaction layers, and on the reaction zone measured in situ by the "atomic probe" method with a field ion microscope using the ionization of desorbed molecules (CO_2) to the gas phase in the field $F \sim 2$ V/Å. The model reflects the character of reaction wave propagation and the intensity of CO_2 formation depending on the adsorption layer structure. A sharp wave front of the reaction zone crossing the "atomic probe" hole with a rate of ~100 ms [16, 20].

Platinum: Self-Oscillations and Waves

The field electron microscopy is based on the tunneling of electrons into vacuum from the surface of a sharp Pt tip (~10^3 Å) under the applied negative electric field ($F = 0.3$ V/Å). Emitted electrons accelerate from the tip surface (Fig. 6a) toward a detector consisting of a high-sensitive microchannel plate and a fluorescent screen [18]. The image is recorded with a CCD camera recorder. The FEM image of the tip surface magnified 3×10^5 times, with a resolution of ~20 Å, appears on the microscope display (Fig. 6b). The FEM image of platinum shows that the hemispherical surface of the sharp tip contains a set of nanoplanes with different crystallographic structures: densest (111), (110), and (100); stepped (331); rough (210) and (310), similar in structure and topography to the surface of supported metal nanoparticles. Therefore, sharp tips can be considered as model systems for solving the "structure gap" problem in the study of the nature of active sites in supported catalysts. The stereographic projection of the nanoplanes on the Pt tip surface is shown in Fig. 6b. The studies showed that the electric fields used in the FEM method exert no noticeable effect on the reactions involving O_2 and CO molecules, in agreement with earlier data [21].

The interpretation of the emission images for CO oxidation is based on the difference between the work functions of the adsorbed species in the layer: O_{ads} atoms, $\Delta\varphi = 1.2$ eV; CO_{ads} molecules, $\Delta\varphi = 0.7$ eV. According to the Fowler–Nordheim equation, the large value of the work function ($\Delta\varphi$) induces a sharp decrease in the emission of electrons from the oxygen layer: contrast dark regions corresponding to the O_{ads} layer appear in the emission images [11]. The sharp decrease in the work function by ~0.4 eV observed in CO oxidation ($\theta_O \longrightarrow \theta_{CO}$) is accompanied by an

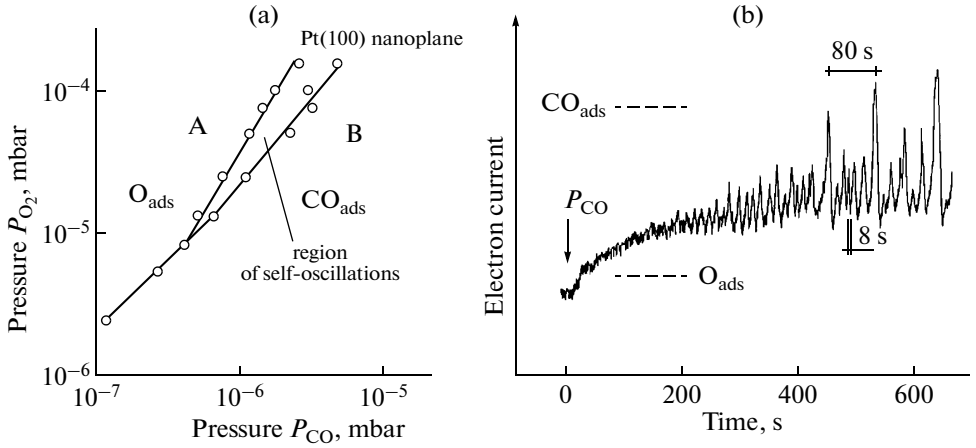

Fig. 7. (a) Kinetic phase diagram of CO oxidation on the Pt(100) nanoplane at 340 K obtained from the conditions of traveling wave formation; (b) the character of origination and periodical change in the electric current from the Pt tip under conditions of self-oscillations of the CO oxidation rate upon the exchange of the adsorption coatings O_{ads} and CO_{ads} with the period of local oscillations $t = 8$ s; $T = 365$ K, $P(O_2) = 5 \times 10^{-4}$ mbar, $P(CO) = 8 \times 10^{-6}$ mbar, $F = 0.4$ V/Å.

increase in electron emission with the appearance of light regions in the image corresponding to the CO_{ads} layer [11]. Figure 6c shows the image of the tip surface with an O_{ads} island on the (100) nanoplane (dark spot) obtained in situ under conditions of traveling wave formation in the CO + O_2 reaction ($T = 450$ K, $P(O_2) = 1.5 \times 10^{-4}$ mbar, $P(CO) = 1 \times 10^{-5}$ mbar) [18]. A characteristic feature of the reaction is the formation of a wave with a sharp boundary between separate CO_{ads} and O_{ads} layers. The interaction of CO with oxygen occurs in the narrow reaction zone (~40 Å) presented in Fig. 6c as a thin light strip along the boundary of the O_{ads} island. The profile of the rate of CO_2 (CO_2^+) formation during wave front propagation in the reaction zone is shown in Fig. 6d. The measurements were taken by field ion mass spectrometry from several metal atoms when the front of the O_{ads} wave crossed the hole of an atom-probe [22]. For the reaction conditions ($T = 450$ K, $P(O_2) = 1.5 \times 10^{-4}$ mbar, $P(CO) = 1 \times 10^{-5}$ mbar), the yield of CO_2 molecules (CO_2^+ ions) has shown a maximum intensity in the reaction zone.

The results of the mass spectrometric measurement of the reaction rate profile indicate a high catalytic activity of platinum in CO_2 formation for the O_{ads} layer. On the contrary, the platinum surface with the adsorbed CO_{ads} layer is inactive due to the blocking of free sites necessary for the dissociative adsorption of O_2.

The kinetic phase diagram with a narrow interval of stable self-oscillations at $T = 340$ K is presented in Fig. 7a. Region A (at $P(O_2) \gg P(CO)$) corresponds to the high activity of platinum with the adsorbed oxygen layer (O_{ads}). Region B corresponds to the low activity of the platinum surface covered by the CO_{ads} layer ($P(O_2) \sim P(CO)$). The catalytically active zone A (O_{ads}) and low-active zone B (CO_{ads}) are separated by a line. At the critical point, at which $P(O_2) = 8 \times 10^{-6}$ mbar and $P(CO) = 7 \times 10^{-7}$ mbar, the line bifurcates to form a region of stable self-oscillations, which coincides well with that for an extended Pt(100) single crystal surface, obtained at a much higher temperature $T = 450$ K [23].

The character of isothermal self-oscillations in CO oxidation on the Pt(100) nanoplane was studied in detail at $T = 365$ K and reactant partial pressures of $P(O_2) = 5 \times 10^{-4}$ mbar and $P(CO) = 8 \times 10^{-6}$ mbar. The origination of stable self-oscillations of electron current, which arise from $O_{ads} \longleftrightarrow CO_{ads}$ changes in the surface coverage with $t \approx 80$ s periodicity, and the origination of rapid local self-oscillations with $t \sim 8$ s on the (100) nanoplane are illustrated in Fig. 7b. The FEM images presented in Figs. 8a–8f characterize different stages of the self-oscillation cycle ($t = 8$ s) of the CO + O_2 reaction:

(a) at $t = 0$, an O_{ads} layer (dark region) is present on the (100), (310), (210), and (110) nanoplanes and a CO_{ads} layer (light region) covers another part of the tip surface formed by the (111), (112), and (113) nanoplanes;

(b) at $t = 2$ s, the (113) and (310) nanoplanes are covered by a CO_{ads} layer (light region), whereas an isolated island of O_{ads} (dark spot at the center of the image) is formed on the unreconstructed nanoplane Pt(100)-(1 × 1);

(c) at $t = 4.1$ s, the very fast "clean-off" CO_{ads} + O_{ads} reaction occurs, resulting in the removal of the oxygen layer; at this reaction stage, the unstable surface (1 × 1) undergoes phase transition to the stable (*hex*) phase, whose clean surface is characterized by a high electron emission intensity (white spot: (*hex*));

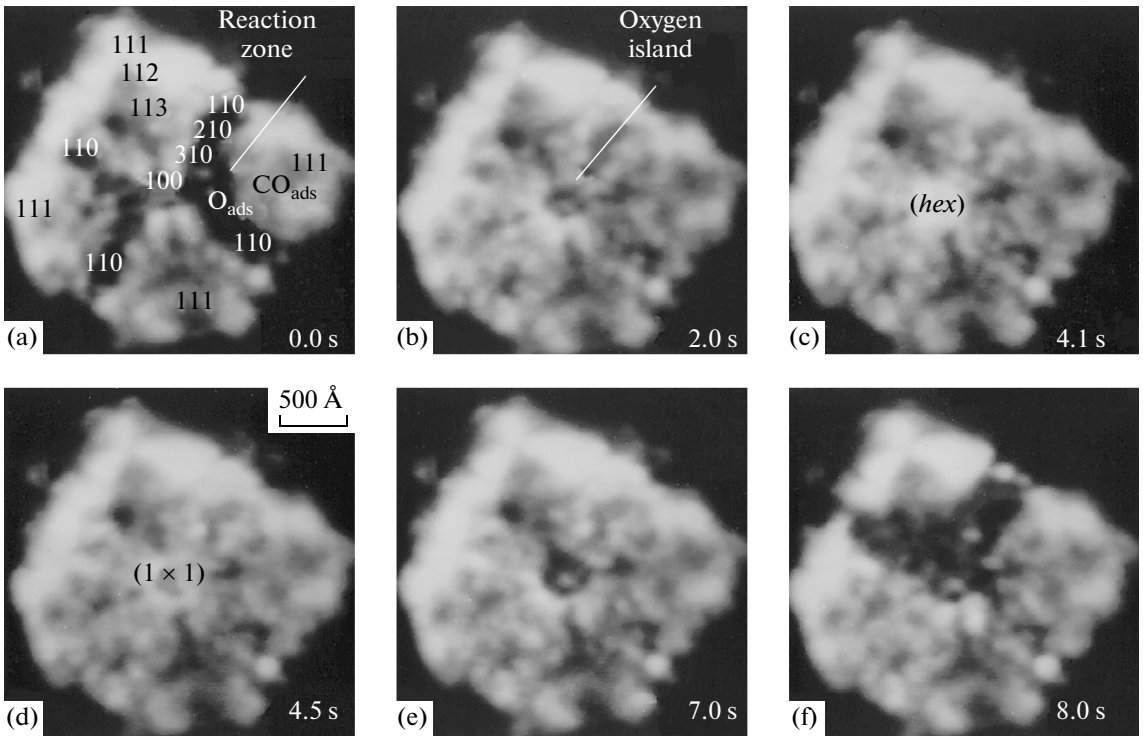

Fig. 8. Sequence of FEM images upon the origination and propagation of regular waves on the Pt(100) nanoplane under conditions of self-oscillations of CO oxidation on the Pt tip ($T = 365$ K, $P(O_2) = 5 \times 10^{-4}$ mbar and $P(CO) = 8 \times 10^{-6}$ mbar, $F =$ 0.4 V/Å). Stereographic projections of the Pt tip with the orientation [100]: (a) at $t = 0$ s, the (100), (310), (210), and (110) nanoplanes are covered with the O_{ads} layer; (b) at $t = 2$ s, the oxygen layer decreases in size with the slow motion of the CO_{ads} wave from the side of the (113), (112), and (111) nanoplanes with the formation of the local island (O_{ads}) on the (100)-(1 × 1) nanoplane; (c) at $t = 4.1$ s, the appearance of the very bright region at the center of the image indicates the formation of the clean surface of the (100) nanoplane in the reconstructed structure (*hex*); (d) at $t = 4.5$ s, CO adsorption is accompanied by the back reconstruction (*hex*) ⟶ (1 × 1); (e) at $t = 7.0$ s, the oxygen island is repeatedly formed on the (100)-(1 × 1) nanoplane; (f) at $t = 8.0$ s, the initial oxygen layer O_{ads} is recovered.

(d) at $t = 4.5$ s, in spite of the high oxygen pressure in the reaction mixture (5×10^{-4} mbar), the low sticking coefficient $S_0(O_2) \sim 10^{-3}$ keeps the (*hex*) surface free of adsorbed oxygen until a local coating with CO_{ads} molecules appears on (*hex*) ($\theta_{CO} \sim 0.1$ ML), again resulting in the reversible phase transition and in the appearance of the (1 × 1) structure (light spot: (1 × 1));

(e) at $t = 7.0$ s, the change in the oxygen sticking coefficient from $S_0(O_2) \sim 10^{-3}$ (*hex*) to $\sim 10^{-1}$ (1 × 1) is accompanied by the reappearance of an O_{ads} island (dark spot);

(f) at $t = 8.0$ s, the (1 × 1) nanoplane initiates the origination of an oxygen wave propagating to the (310), (210), and (110) nanoplanes with the reduction of the primary oxygen layer (a), which completes the autocatalytic cycle.

The results of FEM studies revealed that two spatially separated adlayers (CO_{ads} and O_{ads}) are formed under oscillating conditions. A mobile reaction zone with a width of up to 40 Å and the maximum rate of CO_2 formation was revealed between these coatings. The highly active state of the Pt(100) nanoplane with the (1 × 1) structure is due to both the easy dissociation of oxygen molecules ($S_{1\times1} \sim 10^{-1} \gg S_{hex} \sim 10^{-3}$) and the high reactivity of atomic oxygen (O_{ads}) in CO oxidation. The low activity of the (*hex*) phase is due to the small $S_0(O_2)$ value and the island character of $CO_{1\times1}$ adsorption preventing the dissociation of O_{2ads} molecules.

The theoretical modeling of the spatiotemporal dynamics (self-oscillations, chemical waves) of CO oxidation on the Pt(100) surface using the kinetic Monte Carlo method is based on the reaction mechanism written as the following sequence of steps:

(1) $CO + * \longrightarrow CO_{ads}$ (CO_{hex} or $CO_{1\times1}$),

(2) $CO_{hex} \longrightarrow CO + *_{hex}$,

(3) $CO_{1\times1} \longrightarrow CO + *_{1\times1}$,

(4) (*hex*) ⟶ (1 × 1): $4\,CO_{ads} \longrightarrow 4\,CO_{1\times1}$,

(5) (1 × 1) ⟶ (*hex*): $*_{1\times1} \longrightarrow *_{hex}$,

(6) $O_2 + 2*_{1\times1} \longrightarrow 2O_{1\times1}$,

(7) $O_{1\times1} + CO_{ads} \longrightarrow CO_2 + *_{1\times1} + *$,

(8) $CO_{ads} + * \longrightarrow * + CO_{ads}$.

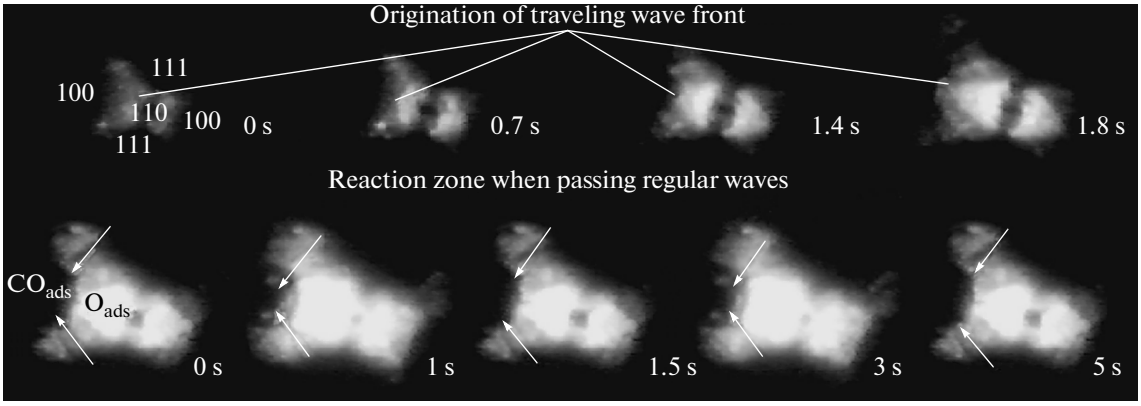

Fig. 9. Sequence of FEM images upon the origination ($t = 0$–1.8 s) and propagation of regular waves (at $t = 0$–5 s) on the Pd(100) nanoplane under conditions of self-oscillations of CO oxidation on the Pd tip ($T = 425$ K, $P(O_2) = 2.6 \times 10^{-3}$ mbar and $P(CO) = 1.3 \times 10^{-4}$ mbar, $F = 0.4$ V/Å. Arrows show the change in sizes of the island of the CO_{ads} molecules localized on the (100) nanoplane. The stereographic projection of the Pd tip with the orientation [110] is shown in the image.

The simulation of the dynamic processes confirms that the maximum rate of CO_2 formation is attained in the narrow reaction zone at the boundary between the O_{ads} and CO_{ads} layers, in agreement with the FEM and FIM data. The propagation of the wave front in the reaction zone results in the achievement of the highest concentration of free sites (necessary for the dissociative adsorption of O_2 molecules), which favors the fast reaction of the O_{ads} atoms with the nearest CO_{ads} molecules [24, 25].

Palladium: Self-Oscillations and Waves

Unlike the Pt(100) face, where self-oscillations are due to the rearrangement of the surface structure, the wave phenomena on the Pd(110) surface are due to purely kinetic effects, specifically, the changes in the catalytic and adsorption properties of the surface, in particular, the oxygen sticking coefficient, due to the comparatively slow formation and depletion of subsurface oxygen: $O_{ads} \longleftrightarrow O_{sub}$ [3, 4]. Isothermal self-oscillations in CO oxidation were studied by FEM on the Pd tip at $T = 425$ K and reactant partial pressures of $P(O_2) = 2.6 \times 10^{-3}$ mbar and $P(CO) = 1.3 \times 10^{-4}$ mbar. Since the change in the work function for the CO_{ads} layer ($\Delta\varphi_{CO} \sim 1$ eV) is higher than that for the O_{ads} layer ($\Delta\varphi_O \sim 0.5$ eV) [26], the maximum intensity of the electron emission current characterizes the oxygen layer (O_{ads}), while the minimum intensity characterizes the CO_{ads} layer.

The FEM images presented in Fig. 9 characterize different stages of the self-oscillation cycle: (1) the origination of the wave front ($t = 0$–1.8 s) and (2) the local character of traveling waves on the Pd tip surface in the region of the (100) nanoplane. At $t = 0$ s, the origination of an oxygen wave (O_{ads}) is initiated on the (110) nanoplane.

The wave front propagates toward the (100) nanoplane, which is followed by the formation on it of an isolated "island" of CO_{ads} molecules ($t = 1.8$ s). Under conditions of the formation of regular waves, the (100) nanoplane region is always covered by a mobile CO_{ads} layer (dark spot indicated by arrows), and the (110) nanoplane region is covered with an O_{ads} layer (light spot). The successive series ($t = 0$ s (CO_{ads}) $\longrightarrow$ 1 s (O_{ads}) $\longrightarrow$ 1.5 s (CO_{ads}) $\longrightarrow$ 3 s (O_{ads}) $\longrightarrow$ 5 s (CO_{ads})) of fast oxygen waves ($t \sim 1.5$ s) shortly interacting with the CO_{ads} layer in a narrow zone of the perimeter of the (100) nanoplane plane within the self-oscillation period ($t \sim 5$ s) is presented in Fig. 9.

Among the so-called "oxide models" proposed for the description of self-oscillations [27], the kinetic model with subsurface oxygen was developed to the greatest extent. In this model, a reversible fourth stage, $O_{ads} \longleftrightarrow O_{sub}$ [28], was added to the three-stage Langmuir–Hinshelwood mechanism. This makes it possible to present the reaction mechanism as two routes (involving atomic (O_{ads}) and subsurface oxygen (O_{sub})) as follows:

Atomic oxygen (O_{ads})

(1) $O_2 + 2* \longrightarrow 2O_{ads}$,

(2) $CO + * \longleftrightarrow CO_{ads}$,

(3) $CO_{ads} + O_{ads} \longrightarrow CO_2 + 2*$,

Subsurface oxygen (O_{sub})

(4) $O_{ads} + *_v \longrightarrow *O_{sub}$,

(5) $CO_{ads} + *O_{sub} \longrightarrow CO_2 + 2* + *_v$,

(6) $CO + *O_{sub} \longleftrightarrow CO_{ads}O_{sub}$,

(7) $CO_{ads}O_{sub} \longrightarrow CO_2 + * + *_v$,

where * and $*_v$ are the active sites of the surface and subsurface layer, respectively. Subsurface oxygen $*O_{sub}$

forms in step (4). The following sequence of stages of the self-oscillation cycle is assumed:

(1) the formation of O_{sub} occurs only on the Pd surface covered with a layer of atomic oxygen O_{ads}, which is accompanied by a decrease in $S_0(O_2)$;

(2) the formation of the CO_{ads} layer is a result of the fast titration reaction $2CO + O_{ads} \longrightarrow CO_2 + CO_{ads}$;

(3) the formation of a high concentration of free adsorption sites is a consequence of the back diffusion of oxygen ($O_{sub} \longrightarrow O_{ads}$) followed by its removal in the form of CO_2;

(4) the reduction of the initial oxygen layer is a result of an increase in $S_0(O_2)$ due to a decrease in the concentration of subsurface oxygen $\theta(O_{sub})$.

The introduction into the four-stage scheme of additional stages (5)–(7), which characterize the possibility of changes in the binding energy of CO_{ads} molecules during the formation of the O_{sub} layer [29], made it possible to describe the formation of spatial-wave structures of different types as solitons, spiral waves, and turbulence on the Pd(110) surface using the kinetic Monte Carlo method [18, 24, 25, 29].

CONCLUSIONS

The character of low-temperature CO oxidation on Pt(100) and Pd(110) single crystal surfaces was established by the HREELS, TPR, and molecular beam techniques. The high catalytic activity of Pt and Pd in the $CO + O_2$ reaction is due to the easy dissociation of molecular oxygen. The studies with the isotope label $^{18}O_{ads}$ suggested that the atomic state of adsorbed oxygen (O_{ads}) is highly reactive in CO_2 formation at low temperatures of 150 to 200 K. The mechanism of low-temperature CO oxidation involving the so-called "hot" oxygen atoms (O_{hot}) was not confirmed. The effect of the concentration of CO_{ads} molecules in the mixed adsorption layer ($O_{ads} + CO_{ads}$) on the reactivity of the atomic form of oxygen resulting in a sharp transition of CO_{ads} oxidation to the low-temperature region ($T < 200$ K) was studied on the Pd(110) surface. This is the low-temperature formation of CO_2 molecules on the Pt(100) surface in CO oxidation that is considered by us as a chemical test for the transition of platinum from the inactive (*hex*) to the highly active catalytic state (1 × 1). Since at $T \sim$ 300–400 K the probability of oxygen dissociation on the Pt(100)-*hex* surface is very low, the appearance of a high concentration of surface defects active in the dissociative adsorption of O_2 during the phase transition (*hex*) $\longrightarrow$ (1 × 1) plays, in our opinion, the key role in the formation of self-oscillations, in the origination and propagation of traveling waves.

The periodical appearance of chemical waves at isothermal self-oscillations of CO oxidation was studied by the FEM method in situ on the Pt and Pd tip surfaces with sizes of about ~10^3 Å. The ability to self-organization of the chemical reaction on the nanoplanes of metals ~200 Å in size through the formation of traveling waves was observed. The character of the phase transitions of the nanoplanes from the lowest active to the highest active surface structures was studied under the self-oscillation conditions. The DFT-calculated values of equilibrium distances and stretching vibration frequencies of twofold bonded oxygen on the Pt(100) surface suggest that the position of the oxygen atom (O_{ads}) in the bridge structure is more preferable compared to adsorption in the on-top or hollow structures.

The following results were observed under the self-oscillation conditions: (1) the initiating role of the reversible phase transition of the Pt(100) nanoplane: (*hex*) $\longleftrightarrow$ (1 × 1); (2) the coexistence of separate regions of CO_{ads} and O_{ads}; (3) the mobile reaction zone up to 40 Å in width with the highest formation rate of CO_2 molecules. It was shown that synchronization between the nanoplanes is achieved by the surface diffusion of CO_{ads} molecules, unlike extended single crystals, for example, in which synchronization during wave propagation occurs through the gas phase. The local character of wave formation in the region of the (100) nanoplane was found and studied on the Pd tip. The mechanism of self-oscillations is related to the reversible formation of the subsurface oxygen layer: $O_{ads} \longleftrightarrow O_{sub}$. The experimental results formed a basis for the modeling of dynamic processes (self-oscillations, waves) by the Monte Carlo method. The most exciting result of this work lies in the following: the appearance of regular waves is an amazing example of self-organization of a catalytic reaction on a metal particle with a size of some hundreds of angströms. Here, self-organization is understood as the spontaneous formation of stable spatiotemporal patterns (chemical waves) in nonequilibrium dissipative media.

ACKNOWLEDGMENTS

This work was supported by the Russian Foundation for Basic Research, project no. 08-03-00454.

REFERENCES

1. Zamaraev, K.I., *Pure Appl. Chem.*, 1997, vol. 69, no. 4, p. 865.
2. Matsushima, T., *Surf. Sci. Rep.*, 2003, vol. 52, nos. 1–2, p. 1.
3. Ertl, G., *Adv. Catal.*, 1990, vol. 37, p. 213.
4. Imbihl, R. and Ertl, G., *Chem. Rev.*, 1995, vol. 95, no. 3, p. 697.
5. Roberts, M.W., *Top. Catal.*, 2005, vol. 36, nos. 1–4, p. 3.
6. Yoshinobu, J. and Kawai, M., *J. Chem. Phys.*, 1995, vol. 103, no. 8, p. 3220.
7. Matsushima, T., *Surf. Sci.*, 1983, vol. 127, no. 3, p. 403.
8. Gorodetskii, V.V., Sametova, A.A., Matveev, A.V, and Bulgakov, N.N., *Khim. Fiz.*, 2007, vol. 26, no. 4, p. 30.

9. Buchachenko, A.L., *Usp. Khim.*, 1999, vol. 68, p. 99.
10. Gorodetskii, V., Block, J.H., Drachsel, W., and Ehsasi, M., *Proc. Post Congr. Symp. "Chemistry of Adsorbed Complexes (Reaction Intermediates) in Catalytic Reaction,"* Szeged, Hungary, 1992.
11. Gorodetskii, V., Block, J.H., Drachsel, W., and Ehsasi, M., *Appl. Surf. Sci.*, 1993, vol. 67, p. 198.
12. Gorodetskii, V., Lauterbach, J., Rotermund, H.-H., Block, J.H., and Ertl, G., *Nature*, 1994, vol. 370, p. 276.
13. Smirnov, M.Yu., Zemlyanov, D., Gorodetskii, V.V., and Vovk, E.I., *Surf. Sci.*, 1998, vol. 414, no. 3, p. 409.
14. Gopinath, C.S. and Zaera, F., *J. Catal.*, 2001, vol. 200, no. 2, p. 270.
15. Gorodetskii, V., Drachsel, W., Ehsasi, M., and Block, J.H., *J. Chem. Phys.*, 1994, vol. 100, no. 9, p. 6915.
16. Gorodetskii, V.V., Sametova, A.A., Matveev, A.V., and Tapilin, V.M., *Catal. Today*, 2009, vol. 144, p. 219.
17. Alavi, A., Hu, P., Deutch, T., Silvestrelli, P.L., and Hutter, J., *Phys. Rev. Lett.*, 1998, vol. 80, nos. 16–20, p. 3650.
18. Gorodetskii, V.V., Elokhin, V.I., Bakker, J.W., and Nieuwenhuys, B.E., *Catal. Today*, 2005, vol. 105, p. 183.
19. Gorodetskii, V.V., Matveev, A.V., Podgornov, E.A., and Zaera, F., *Top. Catal.*, 2005, vol. 32, nos. 1–3, p. 17.
20. Bonzel, H.P., Broden, G., and Pirug, G., *J. Catal.*, 1978, vol. 53, p. 96.
21. Suchorski, Yu., Imbihl, R., and Medvedev, V.K., *Surf. Sci.*, 1998, vol. 401, p. 392.
22. Gorodetskii, V.V. and Drachsel, W., *Appl. Catal., A*, 1999, vol. 188, p. 267.
23. Eiswirth, M. and Schwanker, R., *Z. Phys. Chem.*, 1985, vol. 144, p. 59.
24. Elokhin, V.I., Matveev, A.V., and Gorodetskii, V.V., *Kinet. Katal.*, 2009, vol. 50, no. 1, p. 46 [*Kinet. Catal.* (Engl. Transl.), vol. 50, no. 1, p. 40].
25. Elokhin, V.I., Matveev, A.V., Kovalyov, E.V., and Gorodetskii, V.V., *Chem. Eng. J.*, 2009, vol. 154, nos. 1–3, p. 94.
26. Cobden, P.D., Nieuwenhuys, B.E., and Gorodetskii, V.V., *Appl. Catal., A*, 1999, vol. 188, p. 69.
27. Sales, B.C., Turner, J.E., and Maple, M.B., *Surf. Sci.*, 1982, vol. 114, p. 381.
28. Bassett, M.R. and Imbihl, R., *J. Chem. Phys.*, 1990, vol. 93, p. 811.
29. Elokhin, V.I., Latkin, E.I., Matveev, A.V., and Gorodetskii, V.V., *Kinet. Katal.*, 2003, vol. 44, no. 5, p. 755 [*Kinet. Catal.* (Engl. Transl.), vol. 44, no. 5, p. 692].